A Bioengineered 3-Dimensional Cell Culture Platform Integrated With Microfluidics to Address Antimicrobial Resistance in Tuberculosis

Running title: Bioengineering to combat antimicrobial resistance

Magdalena K Bielecka[1], Liku B Tezera[1], Robert Zmijan[2], Francis Drobniewski[3], Xunli Zhang[2,5], Suwan Jayasinghe[4] and Paul Elkington[1,5]*

[1]NIHR Respiratory Biomedical Research Unit, Clinical and Experimental Sciences Academic Unit, Faculty of Medicine, University of Southampton, UK. [2]Faculty of Engineering, University of Southampton, UK. [3]Department of Infectious Disease, Imperial College London, UK. [4]BioPhysics Group, UCL Institute of Biomedical Engineering, UCL Centre for Stem Cells and Regenerative Medicine and UCL Department of Mechanical Engineering, University College London, UK. [5]Institute for Life Sciences, University of Southampton, UK.

Address for correspondence:

Paul Elkington

Professor of Respiratory Medicine

Clinical and Experimental Sciences

University of Southampton

Southampton SO16 1YD

UK

Tel: 00 44 23 8079 6671

E-mail: p.elkington@soton.ac.uk

Abstract

Antimicrobial resistance presents one of the most significant threats to human health, with the emergence of totally drug-resistant organisms. We combine bioengineering, genetically modified bacteria, longitudinal readouts and fluidics to develop a transformative platform to address the drug development bottleneck, utilising *Mycobacterium tuberculosis* as the model organism. We generate microspheres incorporating virulent reporter bacilli, primary human cells and extracellular matrix using bio-electrospray methodology. Granulomas form within the 3-dimensional matrix and mycobacterial stress genes are up-regulated. Pyrazinamide, a vital first-line antibiotic for treating human tuberculosis, kills *Mycobacterium tuberculosis* in 3-dimensional culture but not in standard 2-D culture or Middlebrook 7H9 broth, demonstrating that antibiotic sensitivity within microspheres reflects conditions in patients. We then perform pharmacokinetic modelling by combining the microsphere system with a microfluidic plate, and demonstrate that we can model the effect of dynamic antibiotic concentrations on mycobacterial killing. The microsphere system is highly tractable, permitting variation of cell content, extracellular matrix, sphere size, infectious dose and surrounding media with the potential to address wide array of human infections and the threat of antimicrobial resistance.

Importance

Antimicrobial resistance is a major global threat and an emerging concept is that infection should be studied in the context of host immune cells. Tuberculosis is a chronic infection which kills over a million people every year and is becoming progressively more resistant to antibiotics. Recent major studies of shorter treatment or new vaccination approaches have not been successful, demonstrating that transformative technologies are required to control tuberculosis. We have developed an entirely new system to study infection of host cells in a 3-dimensional matrix using bioengineering. We show that antibiotics that work in patients are effective in this microsphere system, but not in standard infection systems. We then combine microspheres with microfluidics to model drug concentration changes in patients and demonstrate the effect of increasing antibiotic concentration on bacterial survival. This system can be widely applied to address the threat of antimicrobial resistance and develop new treatments.

Keywords: bioengineering, microfluidics, extracellular matrix, antimicrobial resistance, tuberculosis

Introduction

The progressive emergence of drug-resistant bacteria poses one of the most pressing threats to human health, with the development of totally resistant bacteria potentially leading to a return to the pre-antibiotic era (1-3). The pipeline of new antibiotics in development is inadequate to combat the rate of evolution of microbial resistance (4, 5). To develop antibiotics, bacteria have traditionally been studied in broth culture, where bacilli are rapidly dividing under optimal growth conditions. However, an emerging concept is that studying pathogens in context of the host is vital to fully understand pathogenesis (6, 7). Interaction with host cells modulates multiple facets of bacterial physiology and causes stress-induced changes in bacterial gene expression (8). In parallel, evidence is accumulating that host cell biology is modulated by 3-dimensional extracellular matrix interactions, regulating key processes in the host-pathogen interaction such as cell survival, phagolysosomal fusion, autophagy and cytokine section (9, 10). In patients being treated for infection, the host-pathogen interaction occurs in 3 dimensions and antibiotic concentrations vary over time according to drug pharmacokinetics (11). Conversely, the vast majority of *in vitro* studies are done in the absence of human cells, without extracellular matrix and at static antibiotic concentrations.

Considering these concepts together, we concluded that a transformative system to address the threat of antimicrobial resistance requires the following elements: primary host cells infected with fully virulent bacteria, cultured within a 3-dimensional structure that incorporates physiological extracellular matrix, combined with pharmacokinetic modelling of drug concentrations. These criteria represent a significant challenge in the context of virulent organisms due to the high biosafety containment required and the complexity of bacteria being eluted under flow conditions. We utilised *Mycobacterium tuberculosis* (Mtb), a pathogen that is inherently resistant to antibiotics and causes tuberculosis (TB) (12), to

develop a system that addresses these technical obstacles, and have recently reported investigation of the host immune response in this system (13).

TB is the leading cause of death worldwide from an infectious disease (14) and over the last 2 decades multi-drug resistant (MDR), extensively-drug resistant (XDR) and totally-drug resistant (TDR) strains have sequentially emerged, posing the spectre of completely untreatable disease (15). Unfortunately, major recent trials of novel treatment-shortening regimens have not been successful (16), indicating that the model systems were used to inform these approaches do not sufficiently reflect disease in man. Furthermore, pyrazinamide (PZA), one of the most critical antibiotics in human TB treatment, would not have been discovered by current screening approaches. Current models are principally reliant on microbiological broth or solid media culture, 2-D culture, zebrafish and mice (17). Novel PZA-based regimens show promise (18) and so reliably understanding PZA action has become of critical, principally focused on mutational analysis of PZA resistance (19). These approaches have limitations especially in the context of PZA's complex activation, intracellular activity and uncertain mode of action. For some other drugs, such as cycloserine, nearly all drug susceptibility systems are unreliable. Mtb is an obligate pathogen of man and has a prolonged interaction with host cells, centred on adaption to survival within an intracellular niche (20). In addition, the host-pathogen interaction is spatially organised (21) and the extracellular matrix influences host cell survival (22), suggesting that a fully humanised system structured in 3-D with extracellular matrix is needed to identify novel treatments for TB.

Therefore, we developed a platform utilising Mtb as the prototype organism. Our system integrated genetically modified virulent reporter bacilli, primary human cells and human extracellular matrix using a bioengineering approach, and combined this with a

multiparameter longitudinal readout. Within this microsphere system, we demonstrate cellular aggregation and up-regulation of mycobacterial stress genes. Critically, pyrazinamide is efficacious in the 3-D microsphere system but not in standard broth or 2-D culture. We then combined microspheres with a microfluidic system to permit pharmacokinetic modelling. We observed more rapid Mtb killing with higher peak antibiotic concentrations, similar to outcomes in patients with TB (23). Therefore, this system models conditions in patients and can be readily applied to a range of drug-resistant organisms to address the global challenge of antimicrobial resistance.

Results

Granulomas develop within microspheres and Mtb stress genes are up-regulated

We incorporated primary human cells, virulent Mtb and type I collagen into 3-dimensional microspheres using bio-electrospray methodology (Supplementary Video S1). Fluorescent staining of monocytes and T cells, followed by infection with mCherry-expressing Mtb, showed distribution of cells and bacteria through the microspheres and early granuloma formation from day 4 (Figure 1A). After 14 days of infection, large cellular aggregates resembling human granulomas developed, while no aggregates formed in uninfected microspheres (Figure 1B). Granuloma formation was associated with evidence of mycobacterial stress. Multiple stress-related genes were up-regulated at day 14 in comparison to Mtb in 7H9 broth culture analyzed by reverse-transcription quantitative real-time PCR (RT-QPCR) (Figure 1C), including *lipF*, the acid stress response gene; *recA* encoding recombinase A, the key mediator of the SOS response to DNA damage; *relA*, the nutrient stress related gene; and *sodA*, the oxidative-stress response gene. By infecting cells with genetically modified luminescent Mtb expressing the Lux operon (24) , bacterial growth could be monitored longitudinally over time within microspheres in a non-destructive manner (Figure 1D).

To determine the localisation of mycobacteria, we studied microspheres longitudinally. We compared extracellular with cell-associated bacteria by decapsulating microspheres and performing differential centrifugation to separate extracellular mycobacteria from those intracellular or cell-adherent. The proportion of cell-associated mycobacteria progressively increased over time analyzed by luminescence or CFUs (Figure 2A and 2B), leading to a 20.7-fold increase in luminescence of cell-associated Mtb relative to extracellular Mtb within

151 microspheres at day 15. Gentamicin treatment in a single experiment demonstrated that cell-
152 associated mycobacteria were almost all intracellular, with no significant reduction in CFU
153 after killing extracellular bacteria. Similarly, the fluorescence of cells infected with GFP-
154 expressing Mtb progressively increased over time (Figure 2C and Supplementary Figure S1),
155 demonstrating intracellular proliferation. Mtb infection did not increase cellular toxicity
156 when measured by the Cytotox Glo 3-D assay, with no significant difference in viability
157 between the two conditions (Figure 2D).
158
159 **Standard antibiotics kill Mtb in all conditions**
160 Having demonstrated granuloma formation and the Mtb stress response within microspheres,
161 we first studied standard first-line antibiotics in 2-D cell culture and the 3-D model to
162 determine the tractability of the model and whether killing efficacy was similar in each
163 condition. Rifampicin, isoniazid and ethambutol were added to cell culture media around
164 spheres at physiological concentrations (1µg/ml, 0.25µg/ml and 4µg/ml, respectively). All
165 three antibiotics inhibited Mtb growth in both 2-D and 3-D cell culture systems (Figure 3A
166 and 3B, antibiotics added at day 6; Supplementary Figure S2, antibiotics added at day 1).
167 Rifampicin was the most efficacious at killing Mtb, and isoniazid was consistently more
168 efficient at controlling Mtb in the 3-D microsphere system than the 2-D cell culture. Mtb
169 growth analyzed by luminescence correlated closely with colony forming units (CFUs) on
170 Middlebrook 7H11 agar (Figure 3C).
171
172 **Pyrazinamide is only efficacious in microspheres and not in broth or 2-D cell culture**
173 Next, we investigated pyrazinamide (PZA), which is a key antibiotic in treating human
174 disease but has a poorly defined mechanism of action, using the concentration described in
175 epithelial cell lining fluid (25). Pyrazinamide had no effect on Mtb growth in 7H9 broth
176 without cells at neutral pH (Figure 4A). In 2-D primary cell culture, pyrazinamide had a

temporary effect but Mtb growth rapidly recovered (Figure 4B). Critically, pyrazinamide killed Mtb in the 3-D microsphere system, with luminescence falling to background levels by day 30, using the same antibiotic preparation that had no effect in broth and transient effect in 2-D (Figure 4C). A similar pattern of efficacy was observed when pyrazinamide was added to cultures on day 1, with pyrazinamide having no effect in 7H9 broth, a temporary effect in 2-D culture but complete control of Mtb growth in microspheres (Supplementary Figure S3). Colony counting on 7H11 agar confirmed the Mtb killing by pyrazinamide had equivalent efficacy to isoniazid and moxifloxacin (Figure 4D and S2D).

Second-line antibiotics are most efficacious in 3-D microspheres

We then examined the effect of the second-line antibiotics, D-cycloserine, moxifloxacin and linezolid, which are of increasing importance with the emergence of drug resistant TB. In 7H9 broth, D-cycloserine at low concentration had a minor inhibitory effect, but at high dose was as effective as moxifloxacin (Figure 5A). In 2-D and 3-D systems, D-cycloserine effectively killed Mtb at low and high concentration (Figure 5B and 5C). Linezolid and moxifloxacin effectively suppressed Mtb growth in all three conditions. Isoniazid, included as a control first-line antibiotic, consistently killed Mtb in 3-D microspheres, but bacterial growth resumed in 7H9 broth and the 2-D system. A similar pattern was observed when antibiotics were added at day 1, although the inhibition of Mtb growth by D-cycloserine was more rapid in microspheres compared to 2-D culture (Supplementary Figure S4). To ensure antibiotics were not having a cytotoxic effect on the host cells, we analyzed viability and found no evidence of cytotoxicity after 21 days of culture compared to media or DMSO controls (Supplementary Figure S5).

Pharmacokinetics modelling by integration with microfluidics

In patients, antibiotic concentrations fluctuate over time, as opposed to static concentrations usually studied in the laboratory. Therefore, we integrated the microspheres system with a microfluidic platform to permit modulation of antibiotic concentration over time to mimic *in vivo* pharmacokinetics in patients during treatment (Figure 6A). We studied rifampicin, as plasma concentrations correlate with treatment outcome (23). We manufactured a microfluidic plate from milled poly(methyl methacrylate) (PMMA), providing each well with two inlets and one outlet, permitting smooth flow of media through the wells containing microspheres (Figure 6B). Initially bacterial luminescence from the 24-well plate was undetectable on the GloMax® Discover plate reader. To overcome this, we used phenol-red free media, optimised microsphere density within wells, and placed a custom-made mirror under the plate. These modifications greatly improved the luminescence readout (Figure 6C and 6D) and were able to monitor bacterial growth from experimental day 0.

To model pharmacokinetics in patients, rifampicin at a concentration range (0.25, 1 or 4µg/ml) was irrigated into wells from day 5, incubated for 6 hours and then washed out to leave minimal antibiotic concentration overnight. A stepwise increase in rifampicin concentration in individual wells produced dose-dependent killing of Mtb (Figure 6E). The highest 6 hour peak rifampicin concentration caused equal Mtb killing to constant 1µg/ml antibiotic, or with irrigation with media with 1µg/ml rifampicin (Supplementary Figure S6A). Luminescence increased overnight in the absence of antibiotics, resulting in a saw-tooth pattern of killing, which did not occur at fixed antibiotic concentration and demonstrated rapid recovery of mycobacterial growth once antibiotic pressure was removed. Colony counts on 7H11 agar confirmed that the luminescence data reflected total bacterial load (Figure S6B).

Discussion

Antimicrobial resistance is rapidly emerging as one of the most pressing challenges to global society (2, 3). Innovative approaches to studying the host-pathogen interaction are urgently needed to identify novel treatment approaches that counter the evolution of drug-resistant bacteria. To achieve this, an emerging paradigm is that bacteria should be studied in the context of the host (6). We hypothesised that a transformative platform will require multiple elements that are not currently available in a single system: virulent reporter bacteria, primary human cells, extracellular matrix, 3-dimensional organisation of the host-pathogen interaction and pharmacokinetic modelling. We combined diverse methodologies, including genetically modified bacteria, primary human cell culture, electrostatic microsphere generation, multi-parameter readouts and microfluidics to develop a platform with all requisite elements that could be used in a biosafety containment level 3 environment. In our investigation of the host immune response, we show that host cell survival is improved in the 3-D microsphere model, cellular aggregates form and host-directed therapies can be studied (13). Here, we investigate the system from the pathogen's perspective and demonstrate that mycobacterial stress genes are up-regulated and key antibiotics used to treat human disease are more efficacious in the microsphere system than in standard culture. The non-destructive readouts permit longitudinal analysis over prolonged periods and real-time pharmacokinetic modelling. This platform has the potential to revolutionise antibiotic discovery, and to replace suboptimal animal model systems based on inappropriate host-pathogen combinations.

Miniaturised organoid systems and lab-on-a-chip technologies are rapidly evolving fields for drug discovery, resulting from the widespread belief that studying individual cells or infectious organisms in isolation does not sufficiently reflect conditions *in vivo* (26, 27). The bio-electrosprayer can to produce large numbers of identical microspheres rapidly in a patient

relevant-model, fulfilling a principal requirement of such a system (28). 2-D systems with flow have been developed to study respiratory epithelial cell infection (29), and while several TB cellular systems have been reported (30-34), none combine 3-D culture, collagen and the potential for high throughput or longitudinal analysis. The microsphere system is highly tractable, with the ability to modulate infectious organism and dose, host cellular content, extracellular matrix, microsphere size and surrounding media dynamically.

The need for new antibiotics for TB is particularly acute, given the progressive emergence of drug resistance, recent disappointments in treatment-shortening regimes and the ongoing global toll of infection (14). Pyrazinamide is one of the most important antibiotics in treating human disease, but was discovered serendipitously in the 1950's, and indeed would have not been found by current screening approaches based on sequentially studying minimal inhibitory concentration in broth culture, murine infections and human disease (17). Pyrazinamide has a complex mechanism of action, requiring intracellular acidification. We demonstrated that Mtb stress genes were up-regulated in microspheres and that pyrazinamide killed Mtb in microspheres at neutral pH but not standard 2-D culture systems, studied at a concentration found in epithelial lining fluid (25). This confirms that within microspheres, bacilli are in a pyrazinamide-sensitive compartment and demonstrates the potential to identify other compounds only active against stressed mycobacteria within the correct microenvironment. Similarly, we found that isoniazid (INH) was consistently more effective in the 3-D system that 2-D, with more rapid fall in luminescence and no failed treatments, supporting the relevance of the model to human TB. Therefore, the system can identify drug resistance in a more clinically relevant fashion and can be used to study novel regimens with variable concentrations in combination rather than single new agents at static concentration.

The microsphere system has potential for high throughput use, as from a single blood donor over 5,000 microspheres can be generated within an hour, and diameter is compatible with a 384-well format. Mycobacterial kill curves during antibiotic treatment of patients suggest that there are diverse populations within patients' lungs (35), and therefore the system can be used to study the separate physiological conditions that drive these within the same experiment, such as the hypoxia and nutritional stress. Encapsulation within microspheres permits integration with a microfluidic system without cells and bacteria being lost during irrigation, resolving a significant technical hurdle for pharmacokinetic studies. We were able to show more rapid killing with increased rifampicin concentration, consistent with findings in patients (23, 36). Microfluidics have been used to develop an array of organ-on-a-chip models (37), but we are not aware of development to study virulent containment level 3 pathogens such as Mtb, which represents additional challenges due to the infectious risk. The hollow fibre model has been used to perform advanced pharmacokinetic modelling but pyrazinamide is only efficacious in this system after acidification to pH 5.8 (38), and so cannot be studied in combination with other agents. Future potential developments for the bio-electrospray platform include dual encapsulation to permit a central lipid-rich caseous core, generating an additional layer of flexibility and modelling drug penetration into necrotic foci (39). Development of the microfluidic plate will permit optimisation of combinations of multiple antibiotics in a fully humanised system, with pharmacokinetic modelling of each antibiotic within wells, to identify the best combinations to go forward to clinical trials (34).

We developed a bioengineered cell culture platform that replicates key features of human disease and incorporates primary human cells, extracellular matrix, 3-dimensional structure, virulent bacteria and pharmacokinetic modelling. The microsphere system is highly tractable,

permitting variation of cell content, extracellular matrix, sphere size, infectious dose and surrounding media with the potential to address wide array of human infections. The system can equally be applied to diverse inflammatory and malignant human disease. Integration with molecular microbiology techniques and CRISP-R gene editing will provide genetically tractable host-pathogen pairings. Therefore, this platform has global applicability to address the thread of antimicrobial resistance and deliver new treatments.

Materials and Methods

Bacterial strains, culture conditions and chemicals

Bioluminescent *Mycobacterium tuberculosis* H37Rv (Mtb Lux) (24) and mCherry-expressing *M. tuberculosis* H37Rv (40) were cultured in Middlebrook 7H9 medium (BD Biosciences, Oxford) supplemented with 10% ADC enrichment (SLS), 0.2% glycerol and 0.02% Tween 80 and with kanamycin (25µg/ml) or hygromycin (50µg/ml), respectively. For all experiments, cultures were grown to optical density of 0.6 (approx. 1x 10^8 CFU/ml). Bacterial growth in 7H9 broth was monitored by luminescence (GloMax® 20/20 Single Tube Luminometer; Promega, UK). Chemicals were purchased from Sigma-Aldrich unless stated otherwise.

Human peripheral blood mononuclear cells isolation and infection

Ethical approval for these studies were provided by the National Research Ethics Service Committee South Central - Southampton A, ref. 13/SC/0043. Peripheral blood mononuclear cells (PBMCs) were isolated from single-donor buffy coats from the National Health Service Blood and Transplant, Southampton, UK. Leukocytes were isolated by density gradient centrifugation over Ficoll-Paque (GE Healthcare Life Sciences, UK). Isolated PBMCs were infected with Mtb Lux at a multiplicity of infection (MOI) of 0.1 and kept overnight at 37°C in 5% CO_2 incubator in RPMI 1640 medium supplemented with 10µg/ml ampicillin, 2mM

glutamine, 25 ug/ml kamycin and 10% FBS (foetal bovine serum; Labtech International Ltd.). The next day, infected PBMCs were transferred from vented flasks to 50ml falcon tubes after detachment with Versene solution (Sigma) for 10 min and scraping. After adding HBSS without Ca/Mg (Gibco), cells were spun at 320xg for 8 min at 4°C and the supernatant decanted. The pelleted cells were re-suspended in appropriate volumes of RPMI 1640 medium supplemented with 10µg/ml ampicillin, 2mM glutamine, 25µg/ml kanamycin and 10% of human AB serum (Sigma), referred to as a complete RPMI medium.

2-D culture

Infected cells were resuspended in 50ml of complete RPMI medium and 1ml equally distributed into 2ml Eppendorfs at a final concentration of 3×10^6 cells/ml. Cultures were incubated at 37°C, 5% CO_2. Mtb luminescence was monitored using GloMax® 20/20 Luminometer. Antibiotics were added at pre-determined time points. For colony counts, cultures were treated with 1% saponin in HBSS and bacteria were plated onto 7H11 agar at serial dilutions. For RT-QPCR analysis, infected cells were plated in 6-well plates at a final concentration of 2.5×10^6 cells/ml.

3-D culture

Infected cells were re-suspended in complete RPMI medium, mixed with sterile alginate-collagen at 1×10^6 cells per ml and injected into the Electrostatic Bead Generator (Nisco, Zurich, Switzerland) to form microspheres via a Harvard syringe driver as described previously (41). After generation, microspheres were equally distributed into 2ml Eppendorfs (microsphere volume 0.4ml), immersed in 1ml of complete RPMI medium and incubated at 37°C 5% CO_2. Mtb luminescence was monitored using GloMax® 20/20 Luminometer. For CFU counts, microspheres were dissolved in 55mM Sodium citrate / 10mM EDTA with 1%

saponin in HBSS and bacteria plated onto 7H11 agar. For RT-QPCR analysis, microspheres were cultured in 50ml falcon tubes (microsphere volume 10ml) in complete RPMI medium.

Immunofluorescence and Confocal Imaging

PBMCs were separated into monocytes and lymphocytes using MACS Cell Separation Columns (Miltenyi Biotec, Surrey, UK). Cells were then labelled with CellTracker Blue or CellTrace™ CFSE (ThermoFisher Scientific, UK) separately according to the manufacturer recommendation before infection with mCherry-expressing *M. tuberculosis* H37Rv (40) at MOI of 0.1. Microspheres were generated and fixed in 4% paraformaldehyde after 4 days. Confocal images were acquired on a Leica TCS SP5 Confocal microscope and processed using Image J 1.5 0d (NIH, USA).

Transcription analysis by RT-QPCR

For bacteria grown in 7H9 broth (OD = 0.25) and 2-D culture, total RNA was extracted by centrifugation at 13000 rpm for 10 min and addition of 500µl RNAprotect Bacteria Reagent (Qiagen). The resuspended pellet was left for 10 min at RT prior to repeat centrifugation and resuspension of the pellet in 1ml of TRIzol (Life Technologies) and stored at -80°C. For 3-D culture, RNAlater solution (Ambion) was used to preserve RNA overnight at 4°C. Cells were decapsulated with 100mM Sodium citrate, centrifuged at 3000 g for 30 min, the pellet re-suspended in 1ml of TRIzol (Life Technologies) and stored at -80°C until use. Thawed samples were transferred to Lysis Matrix B tubes containing 0.1mm silica beads (Q-Biogene) and homogenized in a MagnaLyser instrument (Roche) at 4000 rpm for 5 x 45 sec with incubation on ice for 1 min in between each homogenisation. Samples were centrifuged for 1 min at 16100 g at 4°C and supernatant was transferred to a new Eppendorf tube. After phenol/chloroform extraction, the nucleic acids precipitated with isopropanol and were

washed with 75% ethanol, air-dried for 10-15 min and finally re-suspended in nuclease-free water (Fisher Scientific). Genomic DNA was removed using DNA-*free*™ Kit (AM1906; Ambion) according to manufacturer's instructions. RNA was further purified with Qiagen RNeasy Mini kit (Qiagen), treated with on-column DNase digestion with the RNase-free DNase set (79254; Qiagen), repurified using RNeasy Mini kit, and eluted in 50µl of RNase- and DNase-free water (Fisher Scientific). The first-strand cDNA was synthesized in 10µl reaction volumes using the High Capacity cDNA Reverse Transcription Kit (Applied Biosystems). The cDNA samples were diluted 1:3 in nuclease-free water and quantitative real-time PCR was performed in 10µl reaction volumes containing FastStart Universal Probe Master with Rox (Roche), LNA-based probe (designed using the Universal ProbeLibrary System Technology; Roche) (Table 1), oligos (Sigma) (Table 1) and 1µl of cDNA preparation. Reactions were run on a 7900HT Fast Real-Time PCR System (Applied Biosystems) using the following programme: 2 min at 50°C, 10 min at 95°C and 40 cycles of 15 s at 95°C and 1 min at 60°C. All samples were amplified in triplicate and threshold cycle (CT) values ≥ 40 were considered negative. Expression data were normalized by *M. tuberculosis* housekeeping gene, *sigA* and relative quantifications were carried out using ΔΔCt method.

Eukaryotic Cell Viability Assay

Microspheres containing PBMCs alone or *Mycobacterium tuberculosis* infected PBMCs were incubated in 96-well plates for 21 days. Cell viability was analyzed at day 21 using the CellTiter-Glo 3-D Cell Viability Assay (Promega) according to the manufacturer's instructions. Luminescence was analyzed by the GloMax® Discover 96 well plate reader (Promega, UK). Lactate dehydrogenase (LDH) release to measure cell toxicity was analyzed by a colorimetric activity assay (Roche, Burgess Hill, United Kingdom).

Analysis of Mtb location

PBMCs were infected with luminescent Mtb and incorporated into microspheres. At pre-defined time points, microspheres were decapsulated and cell-associated Mtb pelleted by centrifugation at 380 g for 8 min as previously described (42-44). At days 7 and 15, additional samples of cell-associated Mtb were treated with 100µg/ml of gentamicin for 90 min at 37°C in 5% CO_2 incubator to remove non-internalised bacteria, followed by a PBS wash. Mycobacterial location was analyzed by measuring luminescence in the supernatant and pellet, and also by colony counting on Middlebrook 7H11 agar. For flow cytometry, PBMCs were infected with GFP-expressing Mtb at MOI of 0.1. Microspheres were made according to the procedure above and on days 0, 1, 4, 7 and 15, microspheres were decapsulated and stained with Anti-human CD14 APC-conjugated antibody (ImmunoTools, Friesoythe, Germany). Cells were fixed with 2% paraformaldehyde and analyzed on a BD Accuri C6 flow cytometer. All events in high forward and side scatter area stained with CD14 were included in the analysis. Flow cytometry data were analyzed with BD Accuri C6 software (Ver 1.0.264.21). Experiments were done for at least two times in triplicate.

Microfluidic system manufacture

The lid template was based on the original plate lid (Berthold Technologies, UK). The lid was manufactured from a 5mm thick PMMA sheet (Weatherall Equipment & Instruments Ltd) by micro milling on a Protomat 100 micro mill (Germany). The tools used for fabrication were: 3.00mm endmill, and 1.59mm drill (ACS Industries UK). The 3.00mm cutting tool was used to cut out the holding sockets for the Iso-Disc syringe filters (PTFE-4-4, D 4mm x 0.45µm, SUPELCO, USA), and to cut out the exact 127.90 x 85.85mm outline of the lid. The inlets for each well were created by drilling pairs of holes through using the 1.59mm drill, followed by insertion of 30mm long, 0.87mm inner and 1.59mm outer diameters, stainless-steel tubing (Swagelok, UK). The stainless-steel tubing was terminated via PTFE tubing (0.75mm inner diameter) to luer-lock syringe connectors. The outlet port was designed to accommodate the

Iso-Disc syringe filter. Three 0.15mm holes were drilled through each Iso-Disc syringe filter to allow for withdrawal of the liquid from each well during experiments using a 1ml syringe (via the outlet port).

Microfluidic experiments

For microfluidics experiments, microspheres were placed in 24-well plates (Berthold Technologies, UK) with RPMI without phenol red (Gibco), supplemented with 10µg/ml ampicillin, 2mM glutamine, 25µg/ml kanamycin and 10% human AB serum (Sigma). Mtb Lux luminescence was monitored using GloMax® Discover plate reader (Promega, UK). Rifampicin was added to cultures at either day 4 or 5. At 9am each day, wells were treated with different doses of antibiotic and, after 6 hours, wells irrigated 5 times with RPMI. A custom-made mirror was placed under the 24-well clear bottom plate to maximise luminescence collection for detection.

Statistical Analysis

Statistical analyses were preformed using Graph Pad Prism. Differences were considered significant at $P < 0.05$.

Acknowledgements

We would like to thank Jennifer Russell and Regina Teo, University of Southampton, for excellent technical assistance. We thank Nuria Andreu and Siouxsie Wiles for providing the Lux expressing Mtb and Tanya Parish for the mCherry-expressing Mtb.

Funding information

This work was supported by the UK Antimicrobial Resistance Cross Council Initiative funded by the Biotechnology and Biological Sciences Research Council and the Medical Research Council MR/N006631/1, the US National Institute for Health R33AI102239 and the UK National Centre for the 3Rs NC/L001039/1. We are grateful to NAMRIP (the Network for AntiMicrobial Resistance and Infection Prevention) for support, including pump-priming funding via NAMRIP's EPSRC grant NAMRA (EP/M027260/1), part of the EPSRC, Network for Antimicrobial Action, 'Bridging the Gap' programme.

Table 1: Primers and probes

Name	5'-3' sequence
lipF-FOR lipF-REV Roche UPL LNA-probe #160	atgagccgctcgaccata gagccggaaacgtgaataag (FAM)-tgccgccg-dark quencher dye
recA-FOR recA-REV Roche UPL LNA-probe #22	aggagaatgcccgcaact cttcttctcgatctcgtcagc (FAM)-tggtggag-dark quencher dye
relA-FOR relA-REV Roche UPL LNA-probe #152	cgcatcatcgaggtgctat cctggattgccaccagaa (FAM)-tcgccgtc-dark quencher dye
sodA-FOR sodA-REV Roche UPL LNA-probe #85	tggccgaatacaccttgc gagatgtgcggttccagtg (FAM)-gacctgga-dark quencher dye
sigA-FOR sigA-REV Roche UPL LNA-probe #133	agctggccaaagagatgga gggcgtattgctggatttc (FAM)-ggagaagg-dark quencher dye

References

1. **Canton R, Morosini MI.** 2011. Emergence and spread of antibiotic resistance following exposure to antibiotics. FEMS Microbiol Rev **35:**977-991.
2. **Davies J, Davies D.** 2010. Origins and evolution of antibiotic resistance. Microbiol Mol Biol Rev **74:**417-433.
3. **WHO.** 2014. Antimicrobial resistance: global report on surveillance 2014. http://www.who.int/drugresistance/documents/surveillancereport/en/. Accessed 01/06/2016.
4. **Bush K, Courvalin P, Dantas G, Davies J, Eisenstein B, Huovinen P, Jacoby GA, Kishony R, Kreiswirth BN, Kutter E, Lerner SA, Levy S, Lewis K, Lomovskaya O, Miller JH, Mobashery S, Piddock LJ, Projan S, Thomas CM, Tomasz A, Tulkens PM, Walsh TR, Watson JD, Witkowski J, Witte W, Wright G, Yeh P, Zgurskaya HI.** 2011. Tackling antibiotic resistance. Nat Rev Microbiol **9:**894-896.
5. **Spellberg B, Bartlett JG, Gilbert DN.** 2013. The future of antibiotics and resistance. N Engl J Med **368:**299-302.
6. **Bhavsar AP, Guttman JA, Finlay BB.** 2007. Manipulation of host-cell pathways by bacterial pathogens. Nature **449:**827-834.
7. **Scortti M, Lacharme-Lora L, Wagner M, Chico-Calero I, Losito P, Vazquez-Boland JA.** 2006. Coexpression of virulence and fosfomycin susceptibility in *Listeria*: molecular basis of an antimicrobial *in vitro-in vivo* paradox. Nat Med **12:**515-517.
8. **Westermann AJ, Gorski SA, Vogel J.** 2012. Dual RNA-seq of pathogen and host. Nat Rev Microbiol **10:**618-630.
9. **Schwartz MA, Chen CS.** 2013. Cell biology. Deconstructing dimensionality. Science **339:**402-404.

10. **Bonnans C, Chou J, Werb Z.** 2014. Remodelling the extracellular matrix in development and disease. Nat Rev Mol Cell Biol **15:**786-801.

11. **Nielsen EI, Friberg LE.** 2013. Pharmacokinetic-pharmacodynamic modeling of antibacterial drugs. Pharmacol Rev **65:**1053-1090.

12. **Eldholm V, Balloux F.** 2016. Antimicrobial Resistance in *Mycobacterium tuberculosis*: The Odd One Out. Trends Microbiol doi:10.1016/j.tim.2016.03.007.

13. **Tezera LB, Bielecka MK, Chancellor A, Reichmann MT, Al Shammari B, Brace P, Batty A, Tocheva A, Jogai S, Marshall BG, Tebruegge M, Jayasinghe SN, Mansour S, Elkington PT.** 2017. Dissection of the host-pathogen interaction in human tuberculosis using a bioengineered 3-dimensional model. *Elife* **6**.

14. **Wallis RS, Maeurer M, Mwaba P, Chakaya J, Rustomjee R, Migliori GB, Marais B, Schito M, Churchyard G, Swaminathan S, Hoelscher M, Zumla A.** 2016. Tuberculosis-advances in development of new drugs, treatment regimens, host-directed therapies, and biomarkers. Lancet Infect Dis **16:**e34-46.

15. **Udwadia ZF.** 2012. MDR, XDR, TDR tuberculosis: ominous progression. Thorax **67:**286-288.

16. **Warner DF, Mizrahi V.** 2014. Shortening treatment for tuberculosis--to basics. N Engl J Med **371:**1642-1643.

17. **Dartois V, Barry CE, 3rd.** 2013. A medicinal chemists' guide to the unique difficulties of lead optimization for tuberculosis. Bioorg Med Chem Lett **23:**4741-4750.

18. **Diacon AH, Dawson R, von Groote-Bidlingmaier F, Symons G, Venter A, Donald PR, van Niekerk C, Everitt D, Hutchings J, Burger DA, Schall R, Mendel CM.** 2015. Bactericidal activity of pyrazinamide and clofazimine alone and in combinations with pretomanid and bedaquiline. Am J Respir Crit Care Med **191:**943-953.

19. **Casali N, Nikolayevskyy V, Balabanova Y, Harris SR, Ignatyeva O, Kontsevaya I, Corander J, Bryant J, Parkhill J, Nejentsev S, Horstmann RD, Brown T, Drobniewski F.** 2014. Evolution and transmission of drug-resistant tuberculosis in a Russian population. Nat Genet **46:**279-286.

20. **Russell DG.** 2011. *Mycobacterium tuberculosis* and the intimate discourse of a chronic infection. Immunol Rev **240:**252-268.

21. **Marakalala MJ, Raju RM, Sharma K, Zhang YJ, Eugenin EA, Prideaux B, Daudelin IB, Chen PY, Booty MG, Kim JH, Eum SY, Via LE, Behar SM, Barry CE, 3rd, Mann M, Dartois V, Rubin EJ.** 2016. Inflammatory signaling in human tuberculosis granulomas is spatially organized. Nat Med **22:**531-538.

22. **Al Shammari B, Shiomi T, Tezera L, Bielecka MK, Workman V, Sathyamoorthy T, Mauri F, Jayasinghe SN, Robertson BD, D'Armiento J, Friedland JS, Elkington PT.** 2015. The Extracellular Matrix Regulates Granuloma Necrosis in Tuberculosis. J Infect Dis **212:**463-473.

23. **Pasipanodya JG, McIlleron H, Burger A, Wash PA, Smith P, Gumbo T.** 2013. Serum drug concentrations predictive of pulmonary tuberculosis outcomes. J Infect Dis **208:**1464-1473.

24. **Andreu N, Zelmer A, Fletcher T, Elkington PT, Ward TH, Ripoll J, Parish T, Bancroft GJ, Schaible U, Robertson BD, Wiles S.** 2010. Optimisation of bioluminescent reporters for use with mycobacteria. PLoS ONE **5:**e10777.

25. **Conte JE, Jr., Golden JA, Duncan S, McKenna E, Zurlinden E.** 1999. Intrapulmonary concentrations of pyrazinamide. Antimicrob Agents Chemother **43:**1329-1333.

26. **Barrila J, Radtke AL, Crabbe A, Sarker SF, Herbst-Kralovetz MM, Ott CM, Nickerson CA.** 2010. Organotypic 3D cell culture models: using the rotating wall vessel to study host-pathogen interactions. Nat Rev Microbiol **8:**791-801.

27. **Liu Y, Tan S, Huang L, Abramovitch RB, Rohde KH, Zimmerman MD, Chen C, Dartois V, VanderVen BC, Russell DG.** 2016. Immune activation of the host cell induces drug tolerance in *Mycobacterium tuberculosis* both *in vitro* and *in vivo*. J Exp Med **213:**809-825.

28. **Neuzi P, Giselbrecht S, Lange K, Huang TJ, Manz A.** 2012. Revisiting lab-on-a-chip technology for drug discovery. Nat Rev Drug Discov **11:**620-632.

29. **Benam KH, Villenave R, Lucchesi C, Varone A, Hubeau C, Lee HH, Alves SE, Salmon M, Ferrante TC, Weaver JC, Bahinski A, Hamilton GA, Ingber DE.** 2016. Small airway-on-a-chip enables analysis of human lung inflammation and drug responses in vitro. Nat Methods **13:**151-157.

30. **Peyron P, Vaubourgeix J, Poquet Y, Levillain F, Botanch C, Bardou F, Daffe M, Emile JF, Marchou B, Cardona PJ, de Chastellier C, Altare F.** 2008. Foamy macrophages from tuberculous patients' granulomas constitute a nutrient-rich reservoir for *M. tuberculosis* persistence. PLoS Pathog **4:**e1000204.

31. **Guirado E, Mbawuike U, Keiser TL, Arcos J, Azad AK, Wang SH, Schlesinger LS.** 2015. Characterization of host and microbial determinants in individuals with latent tuberculosis infection using a human granuloma model. MBio **6:**e02537-02514.

32. **Braian C, Svensson M, Brighenti S, Lerm M, Parasa VR.** 2015. A 3D Human Lung Tissue Model for Functional Studies on *Mycobacterium tuberculosis* Infection. J Vis Exp doi:10.3791/53084.

33. **Kapoor N, Pawar S, Sirakova TD, Deb C, Warren WL, Kolattukudy PE.** 2013. Human Granuloma In Vitro Model, for TB Dormancy and Resuscitation. PLoS ONE **8:**e53657.

34. **Silva A, Lee BY, Clemens DL, Kee T, Ding X, Ho CM, Horwitz MA.** 2016. Output-driven feedback system control platform optimizes combinatorial therapy of

tuberculosis using a macrophage cell culture model. Proc Natl Acad Sci U S A doi:10.1073/pnas.1600812113.

35. **Horsburgh CR, Jr., Barry CE, 3rd, Lange C.** 2015. Treatment of Tuberculosis. N Engl J Med **373:**2149-2160.

36. **Boeree MJ, Diacon AH, Dawson R, Narunsky K, du Bois J, Venter A, Phillips PP, Gillespie SH, McHugh TD, Hoelscher M, Heinrich N, Rehal S, van Soolingen D, van Ingen J, Magis-Escurra C, Burger D, Plemper van Balen G, Aarnoutse RE, Pan AC.** 2015. A dose-ranging trial to optimize the dose of rifampin in the treatment of tuberculosis. Am J Respir Crit Care Med **191:**1058-1065.

37. **Sackmann EK, Fulton AL, Beebe DJ.** 2014. The present and future role of microfluidics in biomedical research. Nature **507:**181-189.

38. **Gumbo T, Dona CS, Meek C, Leff R.** 2009. Pharmacokinetics-pharmacodynamics of pyrazinamide in a novel *in vitro* model of tuberculosis for sterilizing effect: a paradigm for faster assessment of new antituberculosis drugs. Antimicrob Agents Chemother **53:**3197-3204.

39. **Dartois V.** 2014. The path of anti-tuberculosis drugs: from blood to lesions to mycobacterial cells. Nat Rev Microbiol **12:**159-167.

40. **Carroll P, Schreuder LJ, Muwanguzi-Karugaba J, Wiles S, Robertson BD, Ripoll J, Ward TH, Bancroft GJ, Schaible UE, Parish T.** 2010. Sensitive detection of gene expression in mycobacteria under replicating and non-replicating conditions using optimized far-red reporters. PLoS ONE **5:**e9823.

41. **Workman VL, Tezera LB, Elkington PT, Jayasinghe SN.** 2014. Controlled Generation of Microspheres Incorporating Extracellular Matrix Fibrils for Three-Dimensional Cell Culture. Adv Funct Mater **24:**2648-2657.

42. **Bange FC, Brown AM, Jacobs WR, Jr.** 1996. Leucine auxotrophy restricts growth of *Mycobacterium bovis* BCG in macrophages. Infect Immun **64:**1794-1799.

43. **Cho S, Mehra V, Thoma-Uszynski S, Stenger S, Serbina N, Mazzaccaro RJ, Flynn JL, Barnes PF, Southwood S, Celis E, Bloom BR, Modlin RL, Sette A.** 2000. Antimicrobial activity of MHC class I-restricted CD8+ T cells in human tuberculosis. Proc Natl Acad Sci U S A **97:**12210-12215.

44. **Stegelmann F, Bastian M, Swoboda K, Bhat R, Kiessler V, Krensky AM, Roellinghoff M, Modlin RL, Stenger S.** 2005. Coordinate expression of CC chemokine ligand 5, granulysin, and perforin in CD8+ T cells provides a host defense mechanism against *Mycobacterium tuberculosis*. J Immunol **175:**7474-7483.

Figure legends

Fig. 1: Granulomas form within microspheres and Mtb stress genes are up-regulated. **(A)** Cellular distribution within microspheres. Primary human PBMCs were separated and fluorescently stained (monocytes blue, i, T cells green, ii), recombined and infected with mCherry-expressing Mtb (red, iii). Overlay (iv) shows early granuloma development at day 4. **(B)** Large multicellular granulomas form at day 14 in infected microspheres (ii), which are not observed in uninfected microspheres (i), imaged under inverted microscopy. Scale bar 50μm. **(C)** Mtb stress genes are up-regulated in the microsphere model compared to 7H9 broth culture. Expression of four stress-related mycobacterial genes was analyzed by RT-QPCR in microspheres at day 14 day compared to exponentially growing Mtb (OD_{600} = 0.25) in 7H9 broth. ΔΔCt method was used for relative quantification. Data are presented as fold change normalized to *sigA* gene. Data represent mean of three independent experiments ± SEM. **(D)** Mtb growth monitored in microspheres by bacterial luminescence, demonstrating the typical Mtb luminescence kinetic of infected PBMCs within microspheres (black). Uninfected PBMCs in the microspheres do not luminesce (grey).

Fig. 2: Mtb proliferation within microspheres is intracellular. (A, B) PBMCs were infected with luminescent Mtb and incorporated into microspheres. Cells were released by decapsulation and extracellular and cell-associated bacteria separated by differential centrifugation. Open bars; extracellular mycobacteria, chequered bars; cell-associated mycobacteria. Mycobacterial location determined by luminescence and colony counting on 7H11 agar demonstrated that bacterial proliferation was principally cell-associated. **(C)** PBMCs were infected with GFP-expressing Mtb and incorporated into microspheres. Microspheres were decapsulated and Mtb localisation was analyzed by flow cytometry. (i)

Uninfected cells. GFP-Mtb cells on day 0 (ii), day 1 (iii), day 4 (iv), day 7 (v) and day 15 (vi) show progressive intracellular proliferation. Data are from a representative experiment performed on 2 occasions in triplicate. **(D)** Mtb infection does not reduce cell viability within microspheres. Cellular survival was measured by the CellTiter-Glo 3-D Cell Viability Assay. Data demonstrate the mean +/- SEM of an experiment performed in triplicate on 2 occasions. * $p < 0.05$ *** $p < 0.001$ **** $p < 0.0001$.

Fig. 3: Effect of standard anti-tuberculous antibiotics on Mtb growth. Antibiotics were added at day 6 to 2-D PBMC cell culture or the microsphere system and Mtb growth monitored by luminescence; rifampicin (red, 1µg/ml), isoniazid (blue, 0.25µg/ml) and ethambutol (orange, 4µg/ml). Mtb growth was inhibited by all antibiotics in both 2-D cell culture **(A)** and the 3-D model **(B)**. Mtb growth was unaffected in the control sample (black) or addition of DMSO (grey), used as solvent for rifampicin. Crosses (x) indicate background level of luminescence. Black arrow indicates antibitotic addition. Data are mean +/- SEM for an experiment performed in triplicate and representative of 3 separate experiments. **(C)** Mtb luminescence closely correlates with colony forming unit counts on Middlebrook 7H11 agar. Spearman value $r=0.94$, $p < 0.0001$.

Fig. 4: Pyrazinamide kills Mtb in the 3-D model, but not in 7H9 broth or 2-D culture. **(A)** Pyrazinamide has no effect on Mtb growth in 7H9 broth (dark green, 500µg/ml) compared to untreated control (black). **(B)** Pyrazinamide has a brief effect on Mtb growth in 2-D PBMC cell culture at 60µg/ml (light green), 100µg/ml (mid-green) or 500µg/ml (dark green) in comparison to untreated control (black), but Mtb growth rapidly recovers. **(C)** Pyrazinamide kills Mtb in the 3-D system at 500µg/ml (dark green). Minimal killing of Mtb was observed when 60µg/ml (light green) or 100µg/ml (mid-green) of PZA was added, relative to the control sample (black). Crosses (x) indicate background level of luminescence.

Black arrows indicate antibitotic addition. Data are mean +/- SEM for an experiment performed in triplicate and representative of 3 separate experiments. **(D)** Colony counting on 7H11 agar confirms Mtb killing by pyrazinamide. Dilutions of control and 2-D pyrazinamide plates start from 1:10 dilution, while all others plates start from undiluted. Representative plates are shown.

Fig. 5: D-cycloserine has a similar effect on Mtb growth in 2-D and 3-D culture. (A) Mtb in 7H9 broth. D-cycloserine at low concentration (20µg/ml) had a temporary effect on Mtb growth (light purple), similar to isoniazid (INH) 0.25µg/ml (blue). D-cycloserine 200µg/ml killed Mtb more rapidly (dark purple) as effectively as moxifloxacin (brown, 5µg/ml). Linezolid was the most effective second line antibiotic (magenta, 24µg/ml). Diluent DMSO (grey) did not affect Mtb growth relative to 7H9 broth only (black). **(B)** Mtb growth in 2-D PBMC culture. D-cycloserine at both concentrations inhibited Mtb growth (purple), more rapidly than other antibiotics; moxifloxacin (brown, 5µg/ml), linezolid (magenta, 24µg/ml) and isoniazid (blue, 0.25µg/ml). Mtb growth in control sample (black) and with DMSO (grey). **(C)** Mtb growth in 3-D cell culture model. D-cycloserine, linezolid and moxiflocacin have a similar efficacy as in 2-D cell culture (purple), while isonazid (blue) is more consistently bactericidal. Grey (x) lines indicate background level of luminescence. Black arrows indicate a day antibitotics were added. Data are mean +/- SEM for an experiment performed in triplicate and representative of 3 separate experiments.

Fig. 6: Modelling antibiotic pharmacokinetics by integrating microspheres with a microfluidic system. (A) Representation of antibiotic pharmacokinetics in human plasma after daily oral administration during treatment. **(B)** Microfluidic system with 2 input channels and one exit channel for 24-well tissue culture plate. **(C, D)** Placement of a basal mirror doubles detection of Mtb luminescence by the GloMax® Discover plate reader. Luminescence

from infected PBMCs in microspheres in a single well in the absence (no fill) and presence (stripes) of a basal mirror for 24-well (C) or 96-well tissue culture plate (D). **(E)** Modelling of antibiotic concentration profiles with microfluidic system. From day 5 (black arrow), varying peak concentration of antibiotics were introduced for 6 hours via the fluidic system, and then washed out to approximate pharmacokinetics *in vivo*. Increasing rifampicin concentrations progressively accleterated Mtb killing: 0.25µg/ml (salmon), 1µg/ml (bright red), and 4µg/ml (dark red). Black line represents a control sample to which carrier DMSO was added and identical washes performed. Three independent experiments were carried out, a representative experiment is shown.

Supplementary figure legends

Video S1: Generation of microspheres. Alginate has been stained with bromophenol blue to permit visualization during the bio-electrospray process, which is shown in real time.

Figure S1: FACS analysis strategy for GFP-expressing *M. tuberculosis* associated with cells. Microspheres were generated and on days 0, 1, 4, 7 and 15 were decapsulated. Cells were stained for CD14, fixed with 2% paraformaldehyde for 1h and then analyzed on a BD Accuri C6 flow cytometer. All events in high forward and side scatter area gate were then analyzed for CD14 and GFP signal. Columns: **(i)** Gating area: cells confirmed to be viable in preliminary experiments, **(ii)** FL4 channel: CD14 antibody, **(iii)** FL1 channel GFP plotted against SSC, **(iv)** FL1 GFP channel histogram. **(A)** Unstained, uninfected cells. **(B)** Uninfected cells stained by isotype antibody for CD14 antibody showing no incrrease in FL4 channel. **(C)** Uninfected cells stained by anti-CD14 showing increase in FL4 channel. There was only background signal in the FL1 channel, which detects GFP fluorescence. **(D)** PBMCs infected with GFP+ Mtb stained with isotype control antibody. Infection increases FL1 signal (iii) and (iv). **(E)** PBMCs infected with GFP+ Mtb stained with CD14 antibody. A relative decrease in CD14 expression is observed relative to uninfected cells at day 1 (ii). Mtb infection increases FL1 signal. **(F)** Uninfected PBMCs stained for CD14 at day 15. CD14 expression is reduced (ii). **(G)** Infected PBMCs at day 15 show increased CD14 signal (ii) and also progressive increase in number of GFP positive Mtb associated with cells (iii and iv).

Figure S2: Standard antibiotics kill Mtb in 2-D and 3-D systems added on day 1. Rifampicin (red), isoniazid (blue) and ethambutol (orange) were added at 1, 0.25 and 4μg/ml, respectively, at day 1 either to 2-D cell culture (A) or the 3-D microsphere system (B). Mtb

growth was inhibited by all antibiotics. Mtb growth was unaffected in the control sample (black) or by DMSO (grey). 'x' line indicates background level of luminescence. Black arrow indicates antibitotic administration. Data are mean +/- SEM for an experiment performed in triplicate and representative of 3 separate experiments.

Figure S3: Pyrazinamide kills Mtb more effectively in 3-D microspheres than 2-D culture when added on day 1. (A) Pyrazinamide 500µg/ml (dark green) has no effect on Mtb growth in 7H9 broth in comparison to untreated control. **(B)** PZA at concentrations 60µg/ml (light green), 100µg/ml (mid-green) or 500µg/ml (dark green) initially significantly inhibited Mtb growth in 2-D cell culture compared to untreated controls. However, bacterial regrowth occurred, with Mtb luminescence returning to control levels by day 28. **(C)** Pyrazinamide is bactericidal in the 3-D system. Mtb growth was inhibited slightly by low dose pyrazinamide, while 500µg/ml (dark green) was bactericidal. Grey 'x' lines indicate background level of luminescence. Black arrows indicate antibiotic addition. Data are mean +/- SEM for an experiment performed in triplicate and representative of 3 separate experiments. **(D)** Bacteria were plated out on 7H11 agar on day 28. Colony forming counts confirm the luminescence data reflect bacterial load. Note that dilutions of control and 2-D PZA plates start from 1:10 dilution, while other plates start without dilution. Representative plates are shown.

Figure S4: Second line antibiotics kill Mtb more rapidly in 3-D microspheres than 2-D cell culture when added on day 1. (A) Mtb growth in 7H9 broth. D-cycloserine at low (20µg/ml) and high (200µg/ml) concentration (light and dark purple, respectively) inhibit Mtb growth. However, bacterial regrowth occurred with the lower dose. Isoniazid (blue, 0.25µg/ml) had moderate effect on Mtb growth and regrowth occurred. Moxifloxacin (brown, 5µg/ml) and linezolid (magenta, 24µg/ml) were equally effective but with delayed killing in

comparison to high dose D-cycloserine. Mtb growth was unaffected in control samples (black, and grey with DMSO diluent). **(B)** Mtb growth in 2-D cell culture. D-cycloserine at higher dose (dark purple) had equal efficacy in killing Mtb as other tested antibiotics: 5µg/ml moxifloxacin (brown), 24µg/ml linezolid (magenta) and 0.25µg/ml isoniazid (blue). D-cycloserine at lower concentration inhibited Mtb growth but with a delay in comparison to other antibiotics. **(C)** D-cycloserine kills Mtb more rapidly in 3-D cell culture. All antibiotics investigated were similarly effective against Mtb, with rapid killing and no bacterial regrowth. Grey 'x' lines indicate background luminescence. Black arrows indicate antibitotic addition. Data are mean +/- SEM for an experiment performed in triplicate and representative of 3 separate experiments.

Figure S5: Antibiotics do not cause cytotoxicity within microspheres. Cellular cytotoxicity was investigated at day 21 within the 3-D system using the CellTiter-Glo 3-D cell viability assay. No antibiotic significantly changed cellular survival either in the absence of infection (A) or after Mtb infection (B). Similarly, cytotoxicity is not different in infected cells treated with antibiotics when analyzed by LDH release (C).

Figure S6: High dose rifampicin for 6 hours per day has equal efficacy to constant standard antibiotic concentration. (A) Mtb growth inhibition in the microfluidics system by rifampicin at different concentrations: 0.25 (salmon), 1 (bright red) and 4µg/ml (dark red). Constant 1µg/ml rifampicin (blue) or addition of rifampicin at concentration of 1µg/ml without daily washes (chequered box) had equivalent inhibition of Mtb growth to 4µg/ml temporary peak concentration rifampicin, but no overnight regrowth occurred. Control with DMSO (black) and without DMSO (white squares). **(B)** Colony counts on 7H11 agar confirm that luminescence data reflect total Mtb load within microspheres.

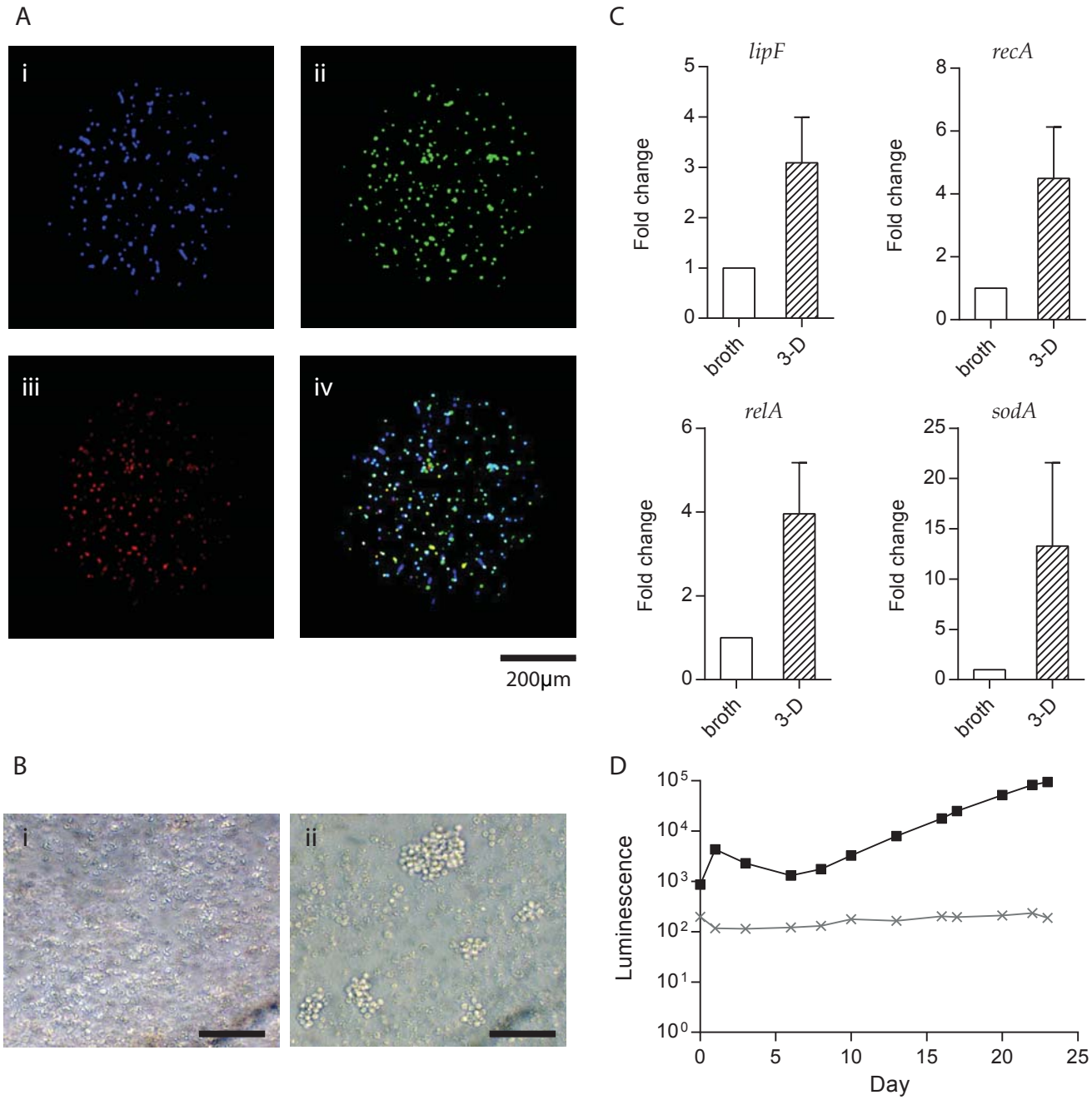

Fig. 1: Granulomas form within microspheres and Mtb stress genes are up-regulated. (A) Cellular distribution within microspheres. Primary human PBMCs were separated and fluorescently stained (monocytes blue, i, T cells green, ii), recombined and infected with mCherry-expressing Mtb (red, iii). Overlay (iv) shows early granuloma development at day 4. **(B)** Large multicellular granulomas form at day 14 in infected microspheres (ii), which are not observed in uninfected microspheres (i), imaged under inverted microscopy. Scale bar 50µm. **(C)** Mtb stress genes are up-regulated in the microsphere model compared to 7H9 broth culture. Expression of four stress-related mycobacterial genes was analysed by RT-QPCR in microspheres at day 14 day compared to exponentially growing Mtb (OD_{600} = 0.25) in 7H9 broth. ΔΔCt method was used for relative quantification. Data are presented as fold change normalized to *sigA* gene. Data represent mean of three independent experiments ± SEM. **(D)** Mtb growth monitored in microspheres by bacterial luminescence, demonstrating the typical Mtb luminescence kinetic of infected PBMCs within microspheres (black). Uninfected PBMCs in the microspheres do not luminesce (grey).

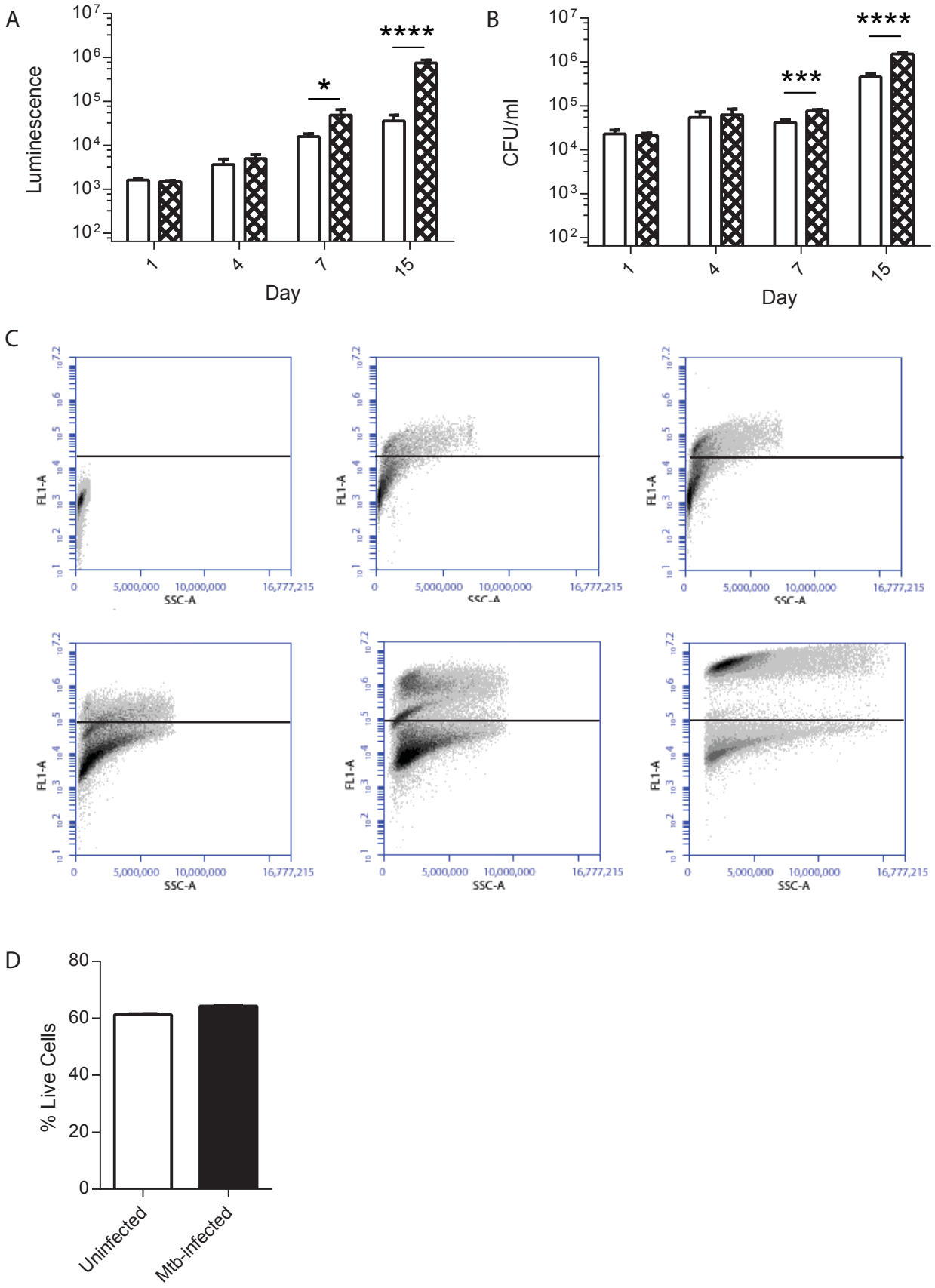

Fig.2: Mtb proliferation within microspheres is intracellular. (A, B) PBMCs were infected with luminescent Mtb and incorporated into microspheres. Cells were released by decapsulation and extracellular and cell-associated bacteria separated by differential centrifugation. Open bars; extracellular mycobacteria, chequered bars; cell-associated mycobacteria. Mycobacterial location determined by luminescence and colony counting on 7H11 agar demonstrated that bacterial proliferation was principally cell-associated. **(C)** PBMCs were infected with GFP expressing Mtb and incorporated into microspheres. Microspheres were decapsulated and Mtb localisation was analyzed by flow cytometry. (i) Uninfected cells. GFP-Mtb cells on day 0 (ii), day 1 (iii), day 4 (iv), day 7 (v) and day 15 (vi) show progressive intracellular proliferation. Data are from a representative experiment performed on 2 occasions in triplicate. **(D)** Mtb infection does not reduce cell viability within microspheres. Cellular survival was measured by the CellTiter-Glo 3-D Cell Viability Assay. Data demonstrate the mean +/- SEM of an experiment performed in triplicate on 2 occasions.

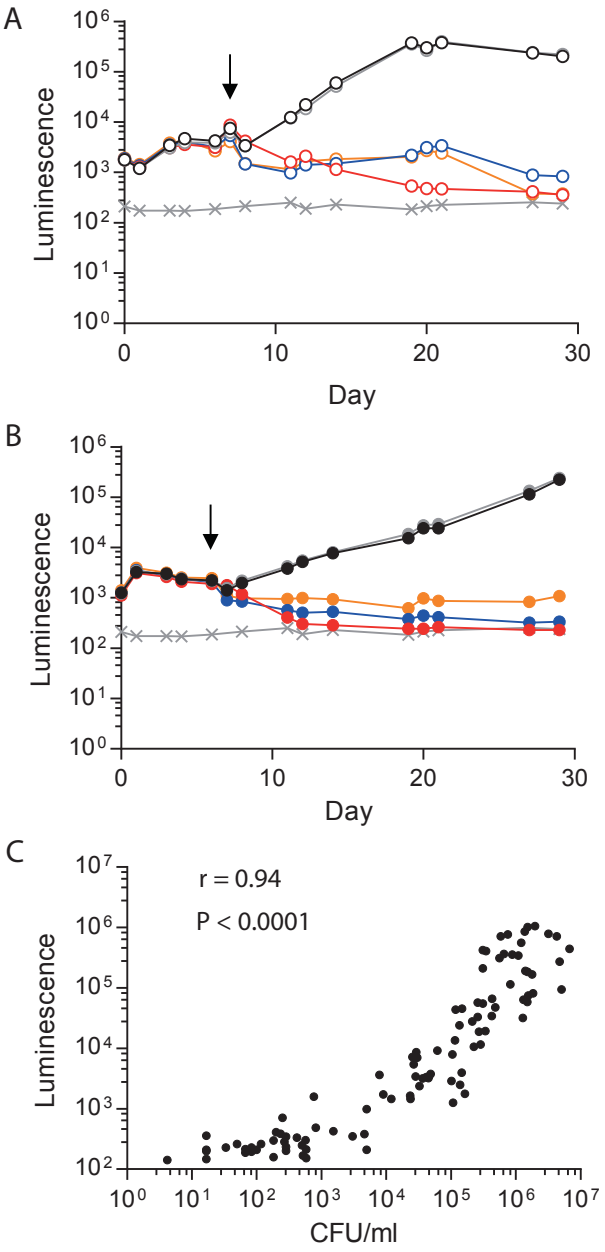

Fig. 3: Effect of standard anti-tuberculous antibiotics on Mtb growth. Antibiotics were added at day 6 to 2-D PBMC cell culture or the microsphere system and Mtb growth monitored by luminescence; rifampicin (red, 1µg/ml), isoniazid (blue, 0.25µg/ml) and ethambutol (orange, 4µg/ml). Mtb growth was inhibited by all antibiotics in both 2-D cell culture **(A)** and the 3-D model **(B)**. Mtb growth was unaffected in the control sample (black) or addition of DMSO (grey), used as solvent for rifampicin. Crosses (x) indicate background level of luminescence. Black arrow indicates antibitotic addition. Data are mean +/- SEM for an experiment performed in triplicate and representative of 3 separate experiments. **(C)** Mtb luminescence closely correlates with colony forming unit counts on Middlebrook 7H11 agar. Spearman value r=0.94, P<0.0001.

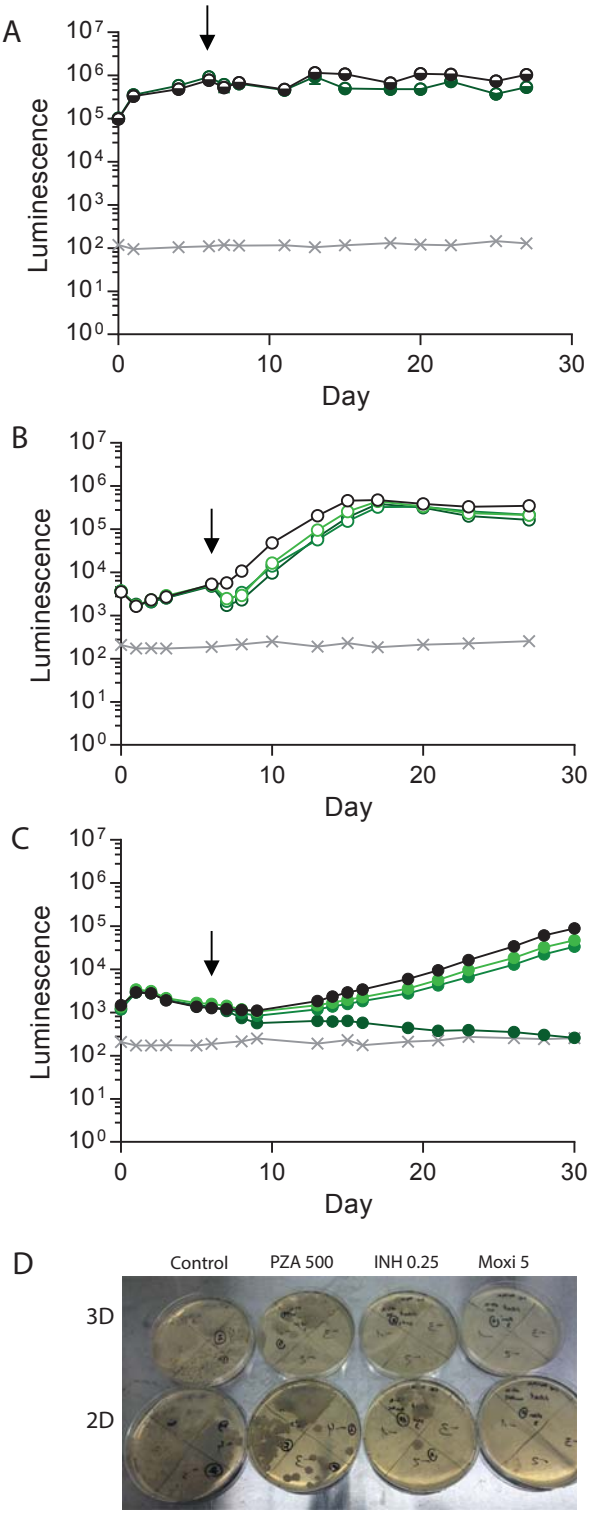

Fig. 4: Pyrazinamide kills Mtb in the 3-D model, but not in 7H9 broth or 2-D culture. (A) Pyrazinamide has no effect on Mtb growth in 7H9 broth (dark green 500µg/ml) compared to untreated control (black). **(B)** Pyrazinamide has a brief effect on Mtb growth in 2-D PBMC cell culture at 60µg/ml (light green), 100µg/ml (mid-green) or 500µg/ml (dark green) in comparison to untreated control (black), but Mtb growth rapidly recovers. **(C)** Pyrazinamide kills Mtb in the 3-D system at 500µg/ml (dark green). Minimal killing of Mtb was observed when 60µg/ml (light green) or 100µg/ml (mid-green) of PZA was added, relative to the control sample (black). Crosses (x) indicate background level of luminescence. Black arrows indicate antibitotic addition. Data are mean +/- SEM for an experiment performed in triplicate and representative of 3 separate experiments. **(D)** Colony counting on 7H11 agar confirms Mtb killing by pyrazinamide. Dilutions of control and 2-D pyrazinamide plates start from 1:10 dilution, while all others plates start from undiluted. Representative plates are shown.

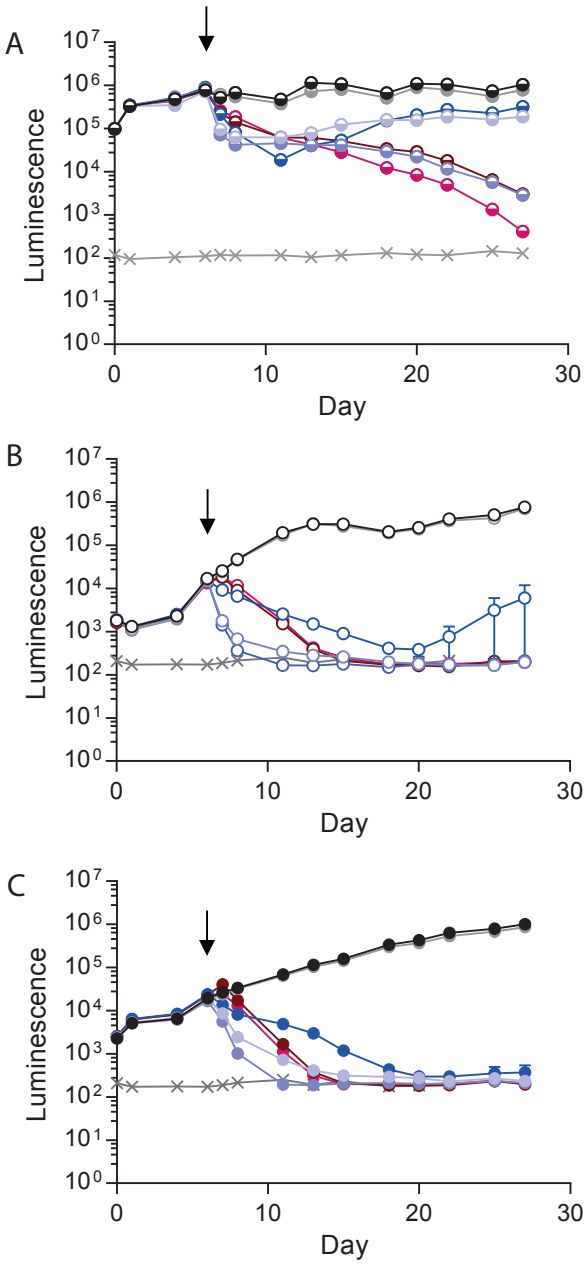

Fig. 5: D-cycloserine has a similar effect on Mtb growth in 2-D and 3-D culture. (A) Mtb in 7H9 broth. D-cycloserine at low concentration (20µg/ml) had a temporary effect on Mtb growth (light purple), similar to isoniazid (INH) 0.25µg/ml (blue). D-cycloserine 200µg/ml killed Mtb more rapidly (dark purple) as effectively as moxifloxacin (5µg/ml, brown). Linezolid was the most effective second line antibiotic (24µg/ml, magenta). Diluent DMSO (grey) did not affect Mtb growth relative to 7H9 broth only (black). **(B)** Mtb growth in 2-D PBMC culture. D-cycloserine at both concentrations inhibited Mtb growth (purple), more rapidly than other antibiotics; moxifloxacin (5µg/ml; brown), linezolid (24µg/ml; magenta) and isoniazid (0.25µg/ml; blue). Mtb growth in control sample (black) and with DMSO (grey). **(C)** Mtb growth in 3-D cell culture model. D-cycloserine, linezolid and moxiflocacin have a similar efficacy as in 2-D cell culture (purple), while isonazid (blue) is more consistently bactericidal. Grey (x) lines indicate background level of luminescence. Black arrows indicate a day antibitotics were added. Data are mean +/- SEM for an experiment performed in triplicate and representative of 3 separate experiments.

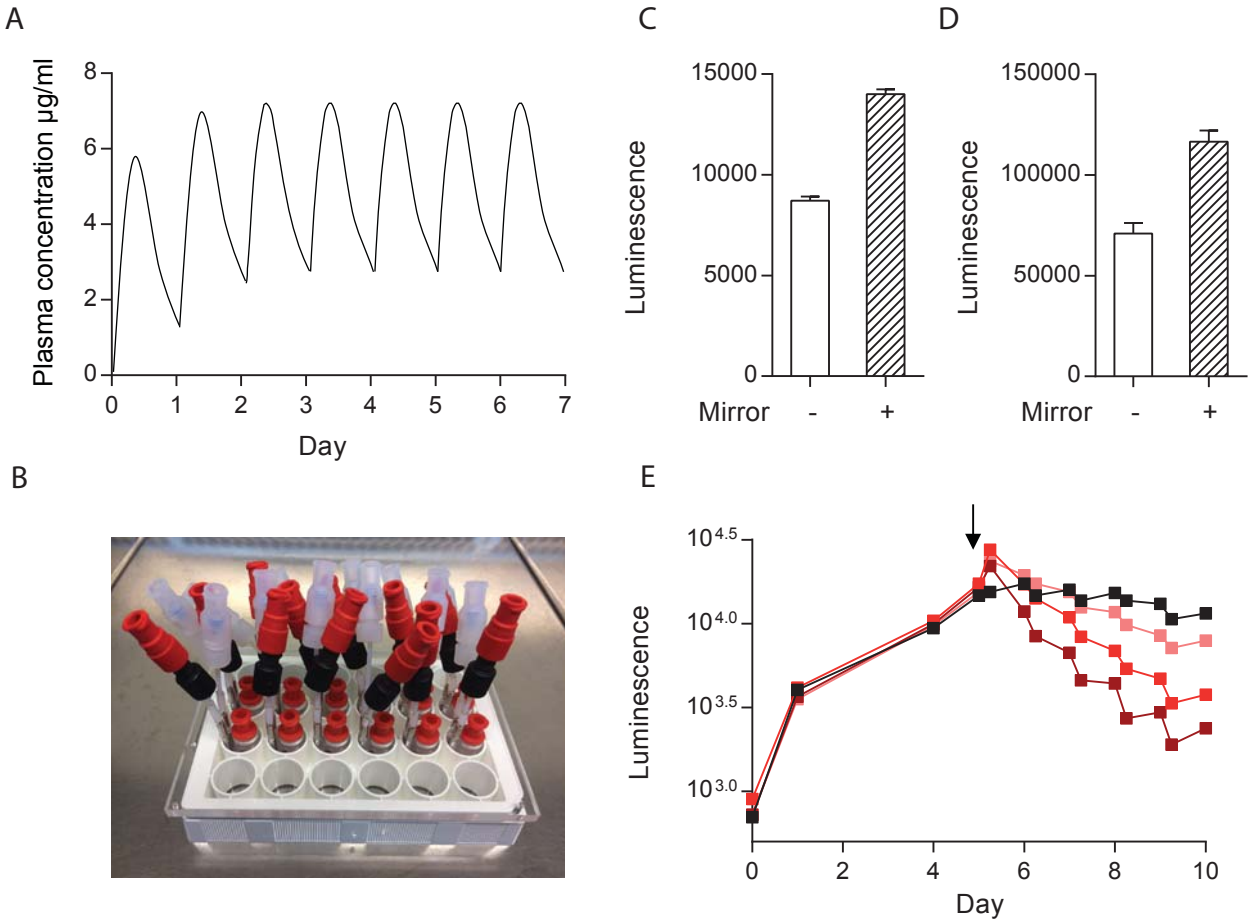

Fig. 6: Modelling antibiotic pharmacokinetics by integrating microspheres with a microfluidic system. (A) Representation of antibiotic pharmacokinetics in human plasma after daily oral administration during treatment. **(B)** Microfluidic system with 2 input channels and one exit channel for 24-well tissue culture plate. **(C, D)** Placement of a basal mirror doubles detection of Mtb luminescence by the GloMax® Discover plate reader. Luminescence from infected PBMCs in microspheres in a single well in the absence (no fill) and presence (stripes) of a basal mirror for 24-well (C) or 96-well tissue culture plate (D). **(E)** Modelling of antibiotic concentration profiles with microfluidic system. From day 5 (black arrow), varying peak concentration of antibiotics were introduced for 6 hours via the fluidic system, and then washed out to approximate pharmacokinetics *in vivo*. Increasing rifampicin concentrations progressively accleterated Mtb killing: 0.25µg/ml (salmon), 1µg/ml (bright red), and 4µg/ml (dark red). Black line represents a control sample to which carrier DMSO was added and identical washes performed. Three independent experiments were carried out, a representative experiment is shown.

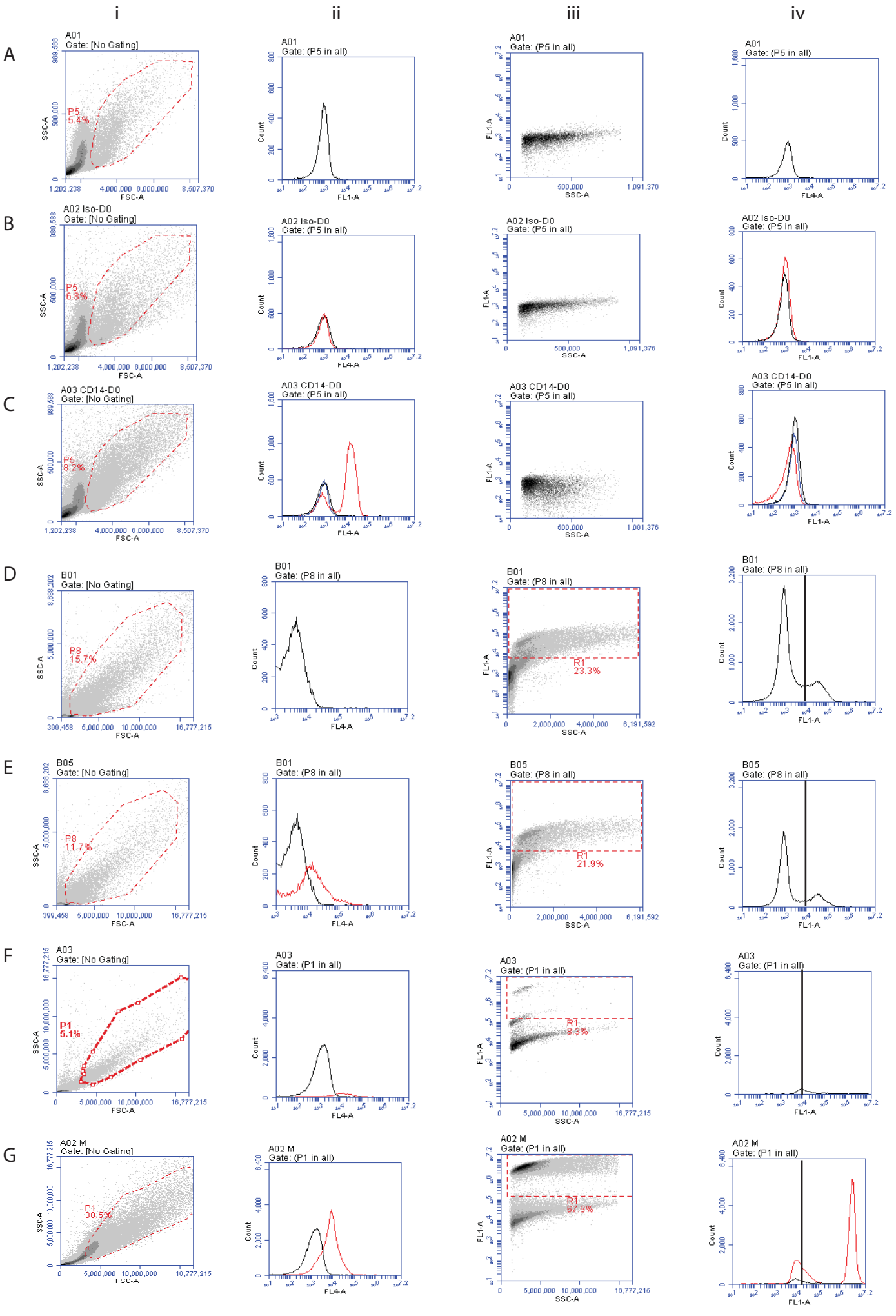

Figure S1: FACS analysis strategy for GFP-expressing *M. tuberculosis* associated with cells.

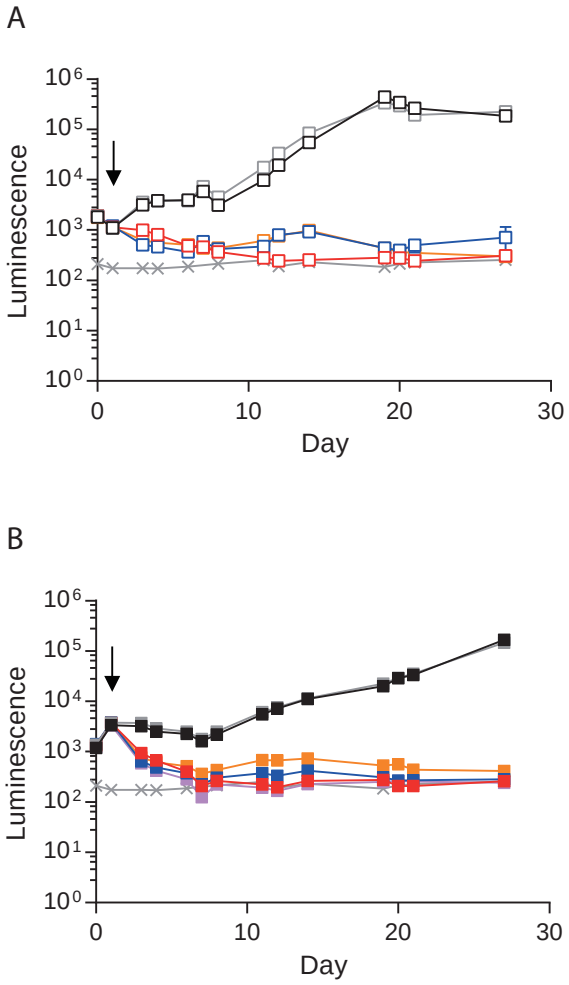

Figure S2: Standard antibiotics kill Mtb in 2-D and 3-D systems added on day 1. Rifampicin (red), isoniazid (blue) and ethambutol (orange) were added at 1, 0.25 and 4µg/ml, respectively, at day 1 either to 2-D cell culture (A) or the 3-D microsphere system (B). Mtb growth was inhibited by all antibiotics. Mtb growth was unaffected in the control sample (black) or by DMSO (grey). 'x' line indicates background level of luminescence. Black arrow indicates antibitotic administration. Data are mean +/- SEM for an experiment performed in triplicate and representative of 3 separate experiments.

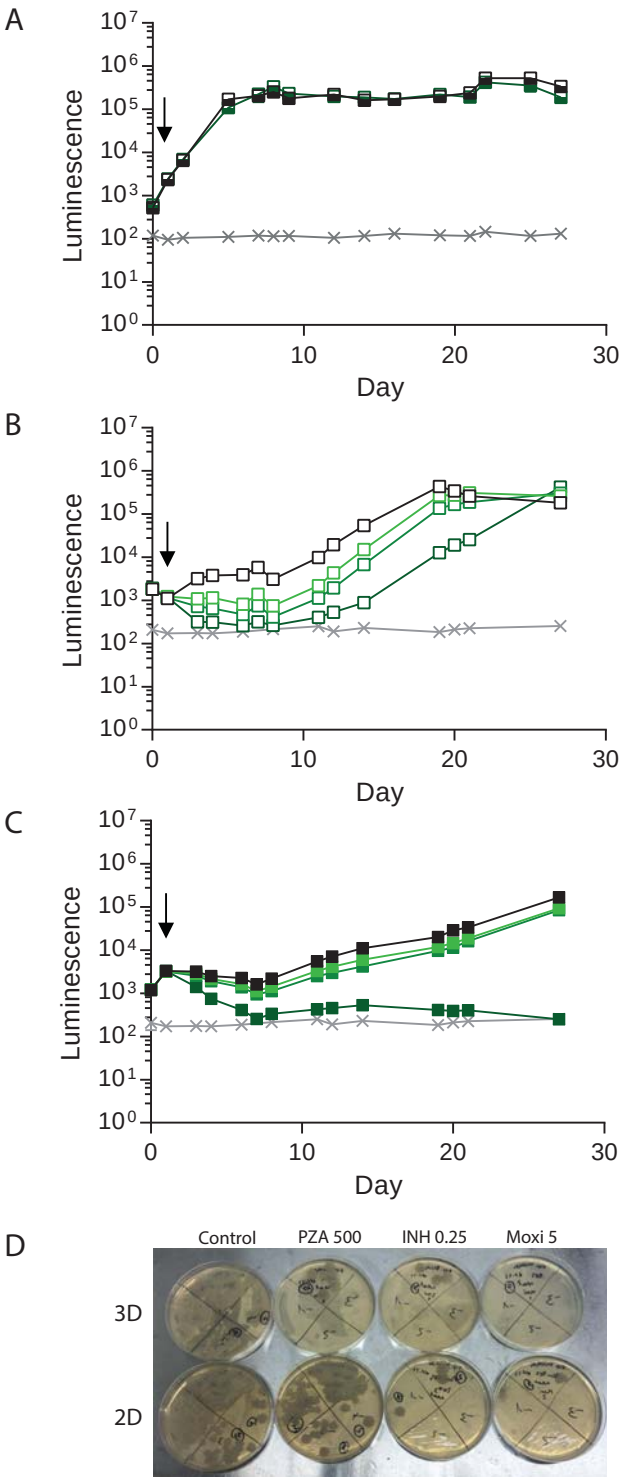

Figure S3: Pyrazinamide kills Mtb more effectively in 3-D microspheres than 2-D culture when added on day 1. **(A)** Pyrazinamide 500µg/ml (dark green) has no effect on Mtb growth in 7H9 broth in comparison to untreated control. **(B)** PZA at concentrations 60µg/ml (light green), 100µg/ml (mid-green) or 500µg/ml (dark green) initially significantly inhibited Mtb growth in 2-D cell culture compared to untreated controls. However, bacterial regrowth occurred, with Mtb luminescence returning to control levels by day 28. **(C)** Pyrazinamide is bactericidal in the 3-D system. Mtb growth was inhibited slightly by low dose pyrazinamide, while 500µg/ml (dark green) was bactericidal. Grey 'x' lines indicate background level of luminescence. Black arrows indicate antibiotic addition. Data are mean +/- SEM for an experiment performed in triplicate and representative of 3 separate experiments. **(D)** Bacteria were plated out on 7H11 agar on day 28. Colony forming counts confirm the luminescence data reflect bacterial load. Note that dilutions of control and 2-D PZA plates start from 1:10 dilution, while other plates start without dilution. Representative plates are shown.

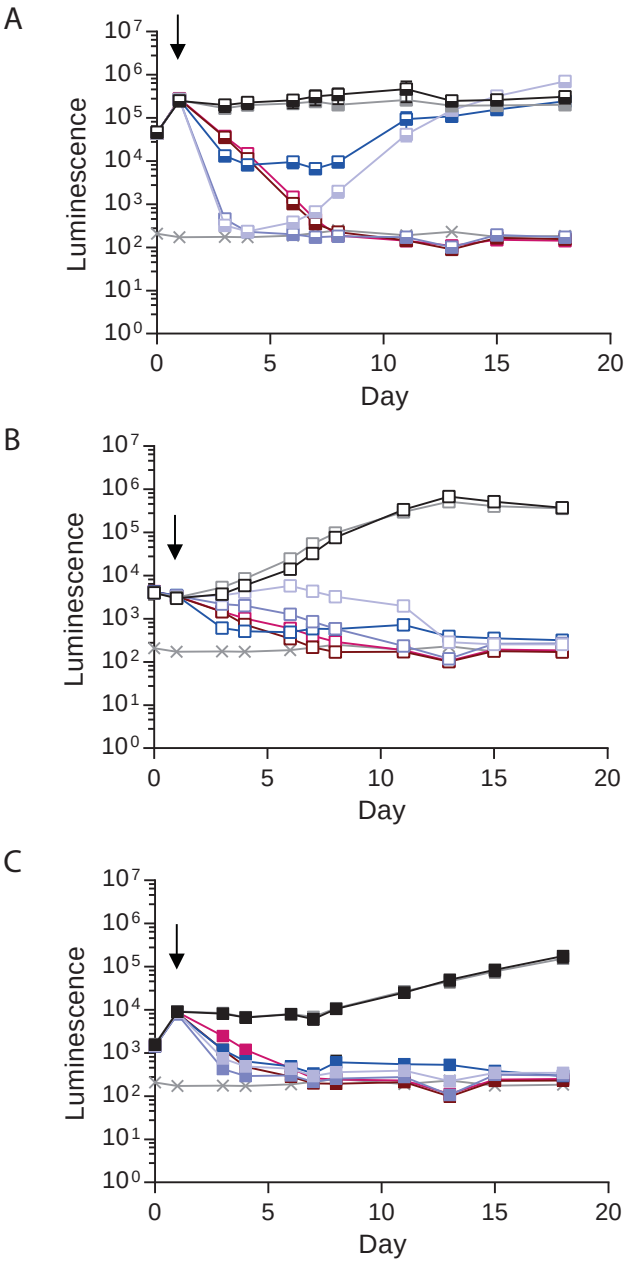

Figure S4: Second line antibiotics kill Mtb more rapidly in 3-D microspheres than 2-D cell culture when added on day 1. (A) Mtb growth in 7H9 broth. D-cycloserine at low (20µg/ml) and high (200µg/ml) concentration (light and dark purple, respectively) inhibit Mtb growth. However, bacterial regrowth occurred with the lower dose. Isoniazid (0.25µg/ml, blue) had moderate effect on Mtb growth and regrowth occurred. Moxifloxacin (5µg/ml, brown) and linezolid (24µg/ml, magenta) were equally effective but with delayed killing in comparison to high dose D-cycloserine. Mtb growth was unaffected in control samples (black, and grey with DMSO diluent). **(B)** Mtb growth in 2-D cell culture. D-cycloserine at higher dose (dark purple) had equal efficacy in killing Mtb as other tested antibiotics: 5µg/ml moxifloxacin (brown), 24µg/ml linezolid (magenta) and 0.25µg/ml isoniazid (blue). D-cycloserine at lower concentration inhibited Mtb growth but with a delay in comparison to other antibiotics. **(C)** D-cycloserine kills Mtb more rapidly in 3-D cell culture. All antibiotics investigated were similarly effective against Mtb, with rapid killing and no bacterial regrowth. Grey 'x' lines indicate background luminescence. Black arrows indicate antibitotic addition. Data are mean +/- SEM for an experiment performed in triplicate and representative of 3 separate experiments.

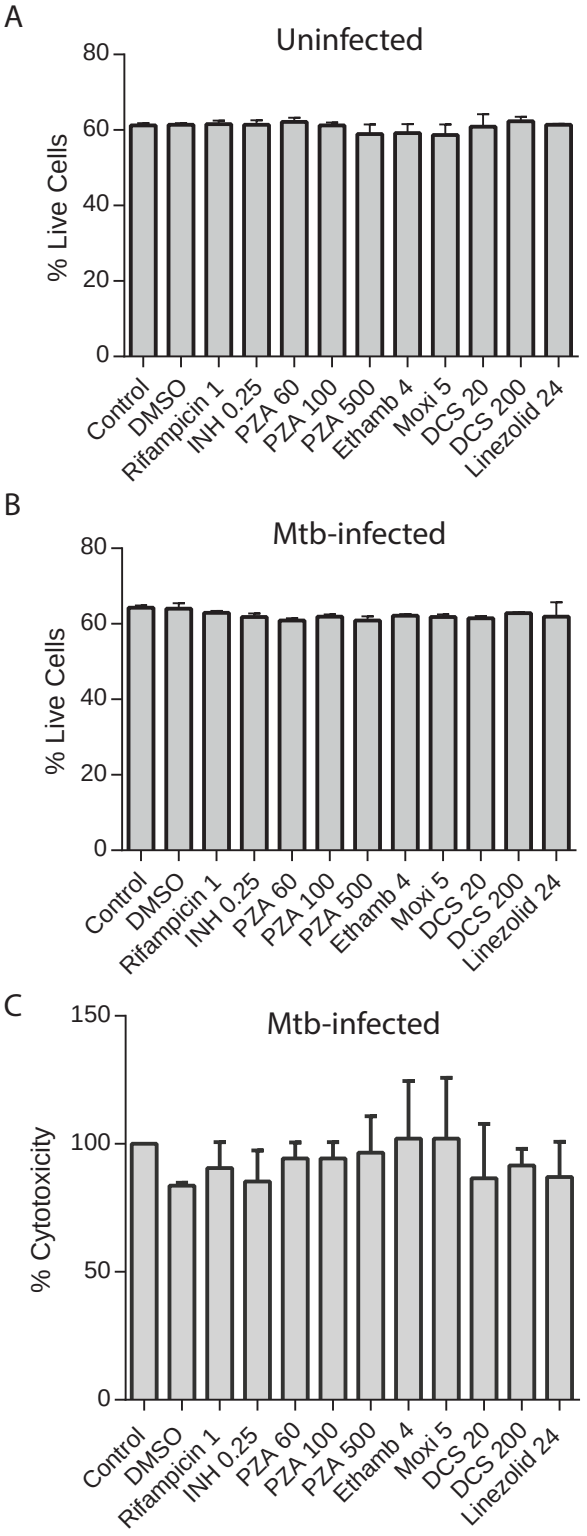

Figure S5: Antibiotics do not cause cytotoxicity within microspheres. Cellular cytotoxicity was investigated at day 21 within the 3-D system using the CellTiter-Glo 3-D cell viability assay. No antibiotic significantly changed cellular survival either in the absence of infection (A) or after Mtb infection (B). Similarly, cytotoxicity is not different in infected cells treated with antibiotics when analyzed by LDH release (C).

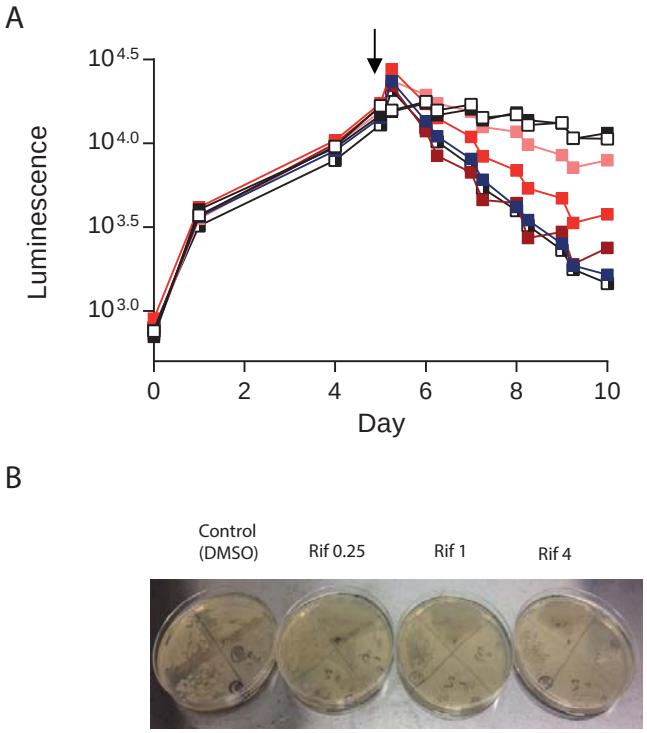

Figure S6: High dose rifampicin for 6 hours per day has equal efficacy to constant standard antibiotic concentration. (A) Mtb growth inhibition in the microfluidics system by rifampicin at different concentrations: 0.25 (salmon), 1 (bright red) and 4µg/ml (dark red). Constant 1µg/ml rifampicin (blue) or addition of rifampicin at concentration of 1µg/ml without daily washes (chequered box) had equivalent inhibition of Mtb growth to 4µg/ml temporary peak concentration rifampicin, but no overnight regrowth occurred. Control with DMSO (black) and without DMSO (white squares). **(B)** Colony counts on 7H11 agar confirm that luminescence data reflect total Mtb load within microspheres.